

Relation among concentrations of incorporated Mn atoms, ionized Mn acceptors and holes in p -(Ga,Mn)As epilayers

R. Moriya and H. Munekata
Imaging Science and Engineering Laboratory
Tokyo Institute of Technology
 4259 Nagatsuta, Midori-ku, Yokohama 226-8503, JAPAN

(Dated: October 29, 2018)

The amount of ionized Mn acceptors in various p -type Mn-doped GaAs epilayers grown at high ($T_s = 580$ C) and low ($T_s = 250$ C) substrate has been evaluated by electrochemical capacitance-voltage measurements, and has been compared systematically with concentrations of incorporated Mn atoms and holes for wide range of Mn concentration ($N_{Mn} = 10^{17} \sim 10^{21} \text{ cm}^{-3}$). Low T_s samples are found to be classified into three different regions: (a) highly resistive, strongly compensated region in $N_{Mn} \leq 10^{18} \text{ cm}^{-3}$, (b) low resistive, fully ionized region in N_{Mn} in between 5×10^{18} and 10^{20} cm^{-3} in which impurity conduction dominates, and (c) magnetic, low-resistive region in $N_{Mn} \geq 2 \times 10^{20} \text{ cm}^{-3}$ in which magnetism and carrier transport are strongly correlated. Quantitative assessment of anomalous Hall effect at room temperature is also carried out for the first time.

PACS numbers: 75.50.Pp, 73.61.Ey, 61.72.Vv, 71.55.Eq

I. INTRODUCTION

(In,Mn)As [1, 2] and (Ga,Mn)As [3, 4], are III-V-based magnetic alloy semiconductors (III-V-MAS) that contain a large amount of magnetic ions. They are usually prepared by molecular beam epitaxy (MBE) at substrate temperatures of 200 – 300 C, which results in suppression of second phases under the condition beyond the equilibrium solubility limit of Mn ($\sim 10^{19} \text{ cm}^{-3}$). They exhibit hole-induced ferromagnetism, and because of this fact, they are expected as one of the strong candidate materials for spintronics devices. Experimental studies on these semiconductors [5, 6] have revealed that they could be described qualitatively as a random alloy in which Mn substitutes for a group III site and takes a dual role of acceptor and local magnetic moment.

Doping of Mn in GaAs up to the equilibrium solubility limit has been studied in 70's. Samples of GaAs:Mn were grown at relatively high temperatures (≥ 560 C) either by MBE or boat-grown method. We call these samples as conventional GaAs:Mn in this paper. In the dilute limit, the level of Mn acceptor was established to be $E_A \approx 110$ meV [7]. Hole concentration could be obtained from low-field Hall effect, through which reduced E_A ($E_A = 60 - 80$ meV) was found with increasing Mn concentration N_{Mn} up to around 10^{19} cm^{-3} [8]. Beyond 10^{19} cm^{-3} , metallic impurity-band conduction took place at low temperatures [9]. Simultaneously, Hall effect deviated from the normal behavior and diminished at low temperatures. Filamental transport characteristics were also inferred. On the other hand, as for the p -type III-V-MAS (Ga,Mn)As grown at relatively low temperatures, ferromagnetic order developed for $N_{Mn} > 4 \times 10^{20} \text{ cm}^{-3}$. Metallic conduction was found in wide range of temperatures for Mn concentrations N_{Mn} ranging $N_{Mn} = 7 - 12 \times 10^{20} \text{ cm}^{-3}$ ($0.03 \leq x \leq 0.05$ in $\text{Ga}_{1-x}\text{Mn}_x\text{As}$) [10], whereas, beyond $N_{Mn} = 12 \times 10^{20} \text{ cm}^{-3}$, non-metallic conduction took place. Magneto-transport was strongly influenced by the magnetic behavior of samples, as exemplified by the anomalous Hall effect [5].

These comparisons raise a question whether (Ga,Mn)As

can be viewed as the extension of conventional Mn doped p -type samples. In order to find answers to this question, development of physical methods that allow us to systematically estimate the concentrations of ionized Mn acceptors N_{Mn^-} and holes p for wide range of Mn concentrations is desired. In particular, determination of N_{Mn^-} and p is important for ferromagnetic samples, since the Curie temperature T_c depends strongly on these quantities [11].

In this work, we are concerned with determination of N_{Mn} , N_{Mn^-} , and p in Mn-doped GaAs epitaxial layers with wide range of Mn concentrations ($10^{17} - 10^{21} \text{ cm}^{-3}$), deposited at low ($T_s = 250$ C) and high ($T_s = 580$ C) substrate temperatures by molecular beam epitaxy. N_{Mn} and p are determined by x-ray diffraction method and low-field Hall effect, respectively. Key experiment is electrochemical $C - V$ method [12]. This method appears to suppress the tunneling current across the thin depletion region in heavily doped samples, and allow us to obtain the amount of Mn incorporated in the form of ionized acceptor without the application of a magnetic field. Carefully comparing N_{Mn^-} with N_{Mn} and p leads us to the following conclusions. For high T_s samples, Mn starts to precipitate as MnAs when N_{Mn} exceeds beyond about $3 \times 10^{18} \text{ cm}^{-3}$. Except this fact, electronic behaviors of epilayers prepared at high T_s are essentially the same as those studied in 70's. For low T_s samples, MnAs precipitates are not found for all the samples studied in this work ($N_{Mn} \leq 1.5 \times 10^{21} \text{ cm}^{-3}$). Electronic behaviors are found to be classified into three different regions. Firstly, (a) highly resistive, strongly compensated region in $N_{Mn} \leq 10^{18} \text{ cm}^{-3}$, and secondly, (b) low-resistive, fully ionized region in $N_{Mn} = 5 \times 10^{18} - 10^{20} \text{ cm}^{-3}$ in which Hall effect virtually disappears. This peculiar behavior is reminiscent of the impurity conduction found in the conventional GaAs:Mn with $N_{Mn} \geq \text{mid } 10^{18} \text{ cm}^{-3}$. In terms of ionization of incorporated Mn, this region shows $N_{Mn} \approx N_{Mn^-}$. The third region is (c) magnetic, low-resistive region in $N_{Mn} \geq 2 \times 10^{20} \text{ cm}^{-3}$ in which magnetism and carrier transport are strongly correlated. Revival of Hall effect in this region suggests the occurrence of electrical conduction through the valence band.

In terms of ionization of Mn, compensation starts to take place again with increasing N_{Mn} . From the relation between N_{Mn} and p in the third region, we quantitatively assess the contribution of anomalous Hall effect at room temperature for the first time for magnetic (Ga,Mn)As.

II. EXPERIMENTAL

Epitaxial layers were grown on semi-insulating GaAs (100) substrates by molecular beam epitaxy. In a growth chamber, a substrate surface was first thermally cleaned at the substrate temperature of $T_s = 600$ C under the As_4 beam flux. Then, a 300-nm-thick GaAs buffer layer was grown at $T_s = 580$ C. This was followed by the growth of either Mn- or Be-doped epitaxial layers. Three different types of epitaxial layers were grown. The first type was Mn-doped layers grown at relatively low T_s of 250 C. The second and third types were Mn- and Be-doped layers grown at $T_s = 580$ C, respectively. The range of Mn and Be concentrations studied in this work were $2 \times 10^{17} - 2 \times 10^{21}$ cm^{-3} and $9 \times 10^{17} - 1 \times 10^{20}$ cm^{-3} , respectively. The ratio of As_4/Ga beam equivalent pressure (BEP) was kept to be 4 - 6 during the epitaxial growth. The growth rate was typically 0.7 $\mu m/hr$, and in any samples, the thickness of the doped layer was kept to be around 0.5 μm .

Mn concentration N_{Mn} of epilayers with $N_{Mn} \geq 1 \times 10^{20}$ cm^{-3} was determined on the basis of the relationship between strain-free cubic lattice constant a_0 and N_{Mn} described in ref.2. A perpendicular lattice constant a_{\perp} was measured by a double-crystal x-ray diffractometer, which was then converted into a_0 assuming that the epilayers were fully compressibly strained. Taking into account the fact that a depends to some extent on the amount of excess As in the epitaxial layers [13], we set the margin of $\pm 0.5 \times 10^{20}$ cm^{-3} for the estimation of N_{Mn} . This margin is also shown as a horizontal bar in the Figs. 3, 4 and 5. As to the relatively low N_{Mn} region ($N_{Mn} < 10^{20}$ cm^{-3}), an equilibrium vapor pressure curve of Mn [14] was used to extrapolate N_{Mn} values from high concentration region. In this case, slight fluctuation of growth rate from MBE run to run was also taken into account for estimating the margin of incorporated Mn concentration. Mn incorporation ratio was assumed to be unity.

Determination of concentration of ionized Mn acceptors N_{A^-} at room temperature was carried out by electrochemical capacitance-voltage (ECV) method. This method, being routinely used in semiconductor laboratories, measures the differential capacitance $C = dQ/dV$ of space charges in semiconductors and related interface [15]. Being analogous to the Schottky junction at the metal-semiconductor interface, the difference in the chemical potential of an electron between an electrolyte solution (ES) and a semiconductor gives rise to charge transfer across the ES-semiconductor interface. This results in the formation of space charge region, being called the depletion region, composed of ionized impurities in a semiconductor. When the amount of interface states is negligibly small and the distribution of ionized impurities is uniform, the capacitance of depletion region for p -type semi-

conductors can be expressed in the following equation:

$$C = \sqrt{\frac{q\epsilon_s(N_{A^-} - N_{D^+})}{V_{bi} - V - \frac{kT}{q}}} \quad (1)$$

Here, q , ϵ_s , $(N_{A^-} - N_{D^+})$, V_{bi} , V , kT are electron charge, relative dielectric constant, the amount of uncompensated charges, built-in barrier height, bias voltage to a semiconductor, and thermal energy, respectively. Impurities whose states E_A are sufficiently less than V_{bi} ($V_{bi} = 0.5 - 0.8$ eV in p -GaAs) are fully ionized in the depletion region. This condition holds for Mn atoms that are incorporated substitutionally, since E_A is 110 meV or less in the doping range of $10^{15} - 10^{19}$ cm^{-3} [7, 8] and satisfies the condition $E_A < V_{bi}$. Therefore, by plotting $1/C^2$ vs V (the Schottky plot), we are able to obtain the concentration of uncompensated ionized Mn acceptors, $N_{A^-} - N_{D^+}$, together with V_{bi} from the slope and the intersection to the x axis, respectively [16].

Measurements were carried out by using a standard electrochemical cell equipped with a saturated calomel reference electrode. p -type surface was placed on an o-ring through which electrical contact with the electrolyte solution of 0.1M $C_6H_2(OH)_2(SO_3Na)_2H_2O$ was established. The contact area was approximately 0.01 cm^2 . A counter ohmic contact to the p -type semiconductor was achieved through soldered indium metal on the surrounding area of the o-ring contact. The frequency ω used in our measurements was varied between 1 and 25 kHz. Frequency dependence on capacitance was fairly small for high T_s samples, whereas it appeared to be not negligibly small for low T_s samples. The $C - V$ region which shows only weak dependence was used for data analysis in the low T_s samples. This point will be discussed in the later section. Depth profile, as carried out by combining electrochemical etching and dQ/dV measurement, showed that all the samples studied in this work have uniform doping profile except for a few-nm-thick top surface region where a native oxide layer exists. Results shown in this paper are based on the data measured after etching samples for the thickness of about 50 nm.

Hole concentration p is estimated from low-field ($H = 0.3$ Tesla) Hall effect measurements at room and liquid-nitrogen temperatures. Van der Pauw method [17] was used for 3-mm square samples. Ohmic contacts were formed by soldering indium at each corner of the sample. In general, Hall resistance R_H for samples incorporating magnetic impurities can be expressed as,

$$R_H = (R_0/d)B + (R_s/d)M \quad (2)$$

$$R_0 = \gamma/ep \quad (3a)$$

$$R_s = c\rho^n \quad (3b)$$

, where R_0 and R_s are ordinary and anomalous Hall coefficients, and B , M , d , ρ , and c are a magnetic field, magnetization, sample thickness, sample resistivity and the constant

associated with asymmetric scattering due to magnetic impurity [18]. In the eq. (3a), the scattering factor γ was assumed to be unity. The power index n in eq. (3b) is either $n = 1$ or 2 for skew or side-jump scattering, respectively. For conventional GaAs:Mn with $N_{Mn} \leq \text{mid } 10^{18} \text{ cm}^{-3}$, p was extracted directly from $R_H = (R_0/d)$, assuming that magnetization was negligibly small. For magnetic (Ga,Mn)As, however, the contribution of the second term in eq. (2) has to be taken into account [3, 5]. It has been demonstrated that the second term can be suppressed when samples are at low temperature (50 mK) with a very high magnetic field (27 Tesla) [19]. This condition, however, is not available routinely in the semiconductor laboratories. Furthermore, it can not be used for highly

resistive and/or paramagnetic samples.

In this study, the contribution of the second term in eq. (2) is evaluated by examining the relation among N_{Mn} , N_{Mn^-} , and p in two ways. The first approach, being applicable for N_{Mn} below the metal-insulating transition, is to examine the consistency among those quantities in view of charge neutrality condition $n + N_{Mn^-} = p$ governed by the Fermi distribution [20]. Experimental values are substituted for N_{Mn} , N_{Mn^-} , and p in eq. (4a) to extract E_A and E_F . If there is mere contribution of the second term in eq. (2), it can be recognized as unreasonable E_A and E_F values that show deviation from those values established by earlier works. The results of this approach are discussed in the section III B.

$$4\pi(2m_e/h^2)^{\frac{3}{2}}F_{\frac{1}{2}}(E_F) + \frac{N_A}{1 + 4\exp(\frac{E_A - E_g - E_F}{kT})} = 4\pi(2m_h/h^2)^{\frac{3}{2}}F_{\frac{1}{2}}[-(E_F + E_g)] \quad (4a)$$

$$F_n(\zeta) = \int_0^{\infty} \frac{E^n dx}{\exp[\frac{E-\zeta}{kT}] + 1}, \quad (4b)$$

The second approach is used for high impurity concentration that is beyond the metal-insulating transition. In this case, impurities are fully ionized and the amount of current carriers is equal to the number of ionized impurities [21]. If there is no contribution of the second term in eq. (2), the p value obtained from the Hall effect measurement should coincide with N_{Mn^-} obtained from $C - V$ method. On the other hand, if we observe the difference between the measured N_{Mn^-} and p values, it can be regarded as the contribution from the second term in eq. (2) and thus the asymmetric scattering. The results of this approach are discussed in the section III C.

III. RESULTS AND DISCUSSION

A. $I - V$ and $C - V$ characteristics

We first show current-voltage ($I - V$) and capacitance-voltage ($C - V$) characteristics of the junction composed of p -GaAs and electrolyte solution. $I - V$ curves in the dark are shown respectively in Figs. 1(a) and (b) for samples grown respectively at high ($T_s = 580 \text{ C}$) and low ($T_s = 250 \text{ C}$) substrate temperatures with various Mn and Be concentrations. The value shown in the x axis is the bias voltage applied to a semiconductor with respect to the reference electrode. It is obvious from both figures that all samples, regardless of dopant species, show rectification characteristics with positive bias being the polarity for a large current. This fact indicates that junctions can be treated as p -type Schottky diodes [16] for which positive bias is the forward direction. In particular, for low T_s samples, the slope of $I - V$ curve in the forward direction increases with increasing the doping concentration, reflecting the enhanced sample conductivity. In

the negative bias region, the tunneling current across the thin depletion region is well suppressed presumably because of the lack of available empty states in an electrolyte solution (ES). Nevertheless, the breakdown voltage in the negative bias region gradually decreases with increasing doping concentration. Extrapolating forward current density to zero-voltage, saturation current can be extracted, from which the zero-field barrier height at the ES/semiconductor interface can be estimated on the basis of thermionic emission model. The barrier heights thus obtained from various samples are centered around $0.62 \pm 0.04 \text{ eV}$. These values are consistent with those reported for conventional metal/ p -GaAs Schottky diodes [22].

Figs. 2(a) shows $1/C^2 - V$ relationships for p -type, high T_s samples ($T_s = 580 \text{ C}$). Linear relationship is clearly seen for wide range of bias voltage. There is almost no ω dependence throughout the entire frequency range (1 – 25 kHz) used in this work. A slope decreases monotonously with increasing doping concentration irrespective of dopant species. The number of ionized Mn, N_{Mn^-} , estimated from eq.(1) coincides well with the incorporated Mn concentration N_{Mn} . The barrier height extracted from the intercept with the x axis is 0.4 - 0.6 eV, being consistent with values obtained from $I - V$ data. These facts indicate that a well defined depletion region is established at an ES/semiconductor junction for samples grown at high T_s .

On the other hand, for low T_s samples ($T_s = 250 \text{ C}$), a straight $1/C^2 - V$ relationship can be established for a limited bias region defined by the bias voltage of - 0.1 V or higher (Fig. 2(b)). As to the negative bias region lower than - 0.1 V, the relationship becomes strongly nonlinear, making it difficult to analyze by the Schottky plot. In an extreme case, as seen for the sample with Mn concentration of $5 \times 10^{19} \text{ cm}^{-3}$,

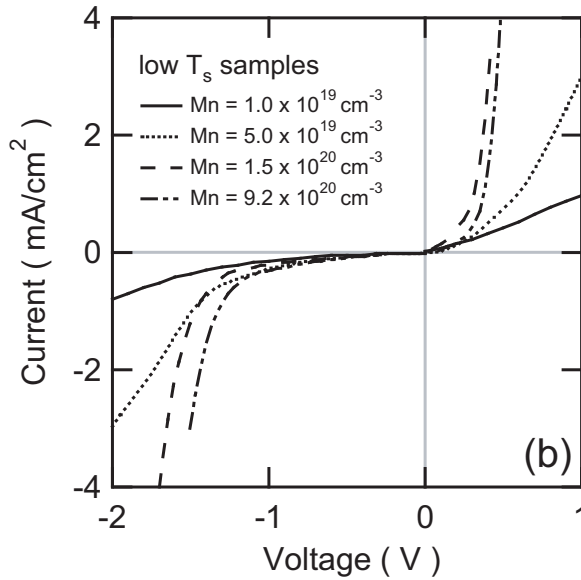
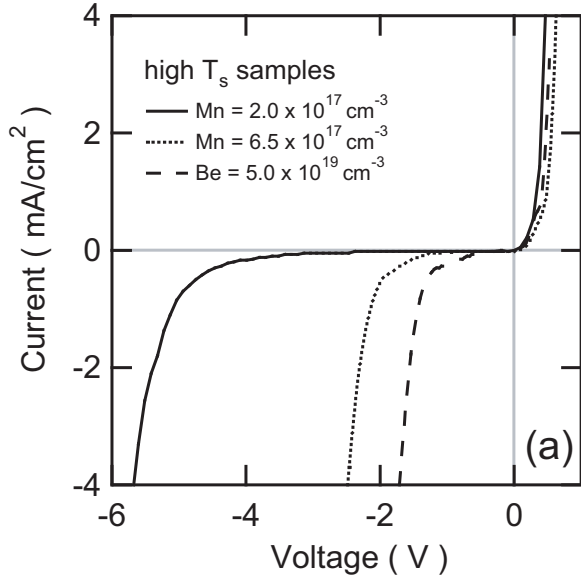


FIG. 1: Current-voltage (I - V) characteristics of various ES/GaAs:X (X =Mn and Be) junctions at room temperature. GaAs:X epitaxial layers were grown by molecular beam epitaxy at substrate temperatures of (a) $T_s = 580$ C (high T_s samples) and (b) $T_s = 250$ C (low T_s samples).

the straight relationship appears just in between 0.3 and 0.4 V. A strong deviation from the linear relationship in the negative bias region, which also occurs for GaAs:Be samples grown at low T_s , is probably due to relatively deep interface/bulk states associated with the low temperature growth. In fact, the nonlinear region is strongly ω dependent ($\omega = 10 - 25$ kHz), whereas the linear region is rather independent of ω . N_{Mn^-} deduced from the linear region matches well with N_{Mn} (Fig. 3). Moreover, the barrier heights extracted from the linear region are around 0.5 – 0.6 eV, being consistent with values extracted from p -type samples grown at high T_s . On the basis of these

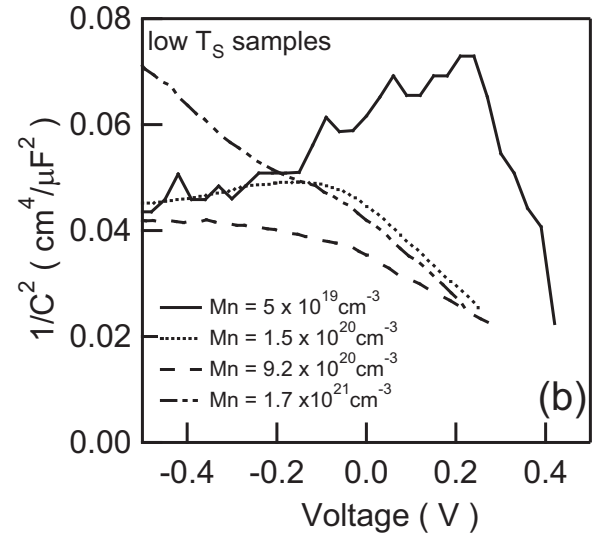
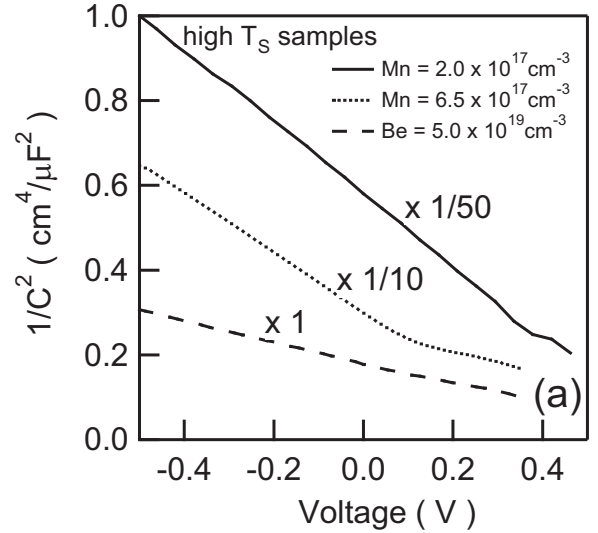


FIG. 2: $1/C^2 - V$ characteristics for ES/GaAs:X (X = Mn and Be) junctions at room temperature. Modulation ac-frequency was 5 kHz. GaAs:X epitaxial layers were grown by molecular beam epitaxy at substrate temperatures of (a) $T_s = 580$ C (high T_s samples) and (b) $T_s = 250$ C (low T_s samples).

findings, we conclude that N_{Mn^-} for low T_s samples can be extracted by carefully analyzing the $C - V$ data. We confirm that the results disclosed recently in rapid communication [12] are convincing.

B. Relation between N_{Mn} and N_{Mn^-}

The relation between N_{Mn} and N_{Mn^-} is summarized in Fig. 3. Open squares and black circles represent N_{Mn^-} values for high and low T_s samples, respectively. A dashed line in the figure depicts the relation $N_{Mn^-} = N_{Mn}$. For high T_s samples, N_{Mn^-} increases monotonously with N_{Mn} up to around the mid range of 10^{18} cm^{-3} with the relation $N_{Mn^-} \approx N_{Mn}$. This

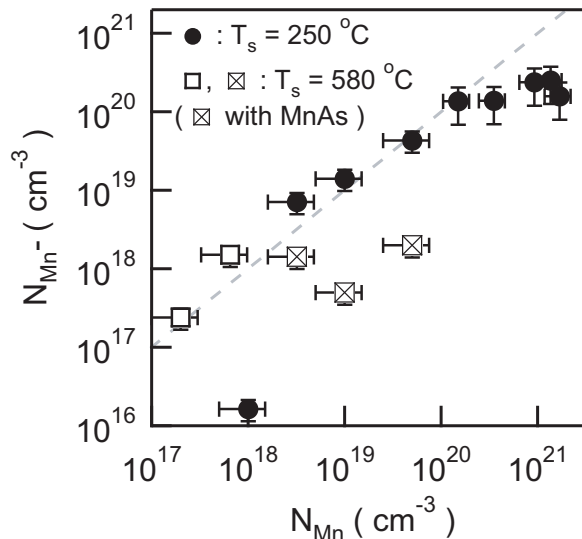


FIG. 3: Relation between incorporated Mn concentration N_{Mn} and ionized Mn acceptor concentration N_{Mn^-} . Dashed line indicates the relation $N_{Mn^-} = N_{Mn}$. and represent N_{Mn^-} values for high and low T_s samples, respectively. \boxtimes represents N_{Mn^-} values for high T_s sample containing MnAs.

fact indicates that incorporated Mn atoms become acceptors and are fully ionized in the depletion region, being consistent with the works done in 70's. For N_{Mn} higher than mid 10^{18} cm^{-3} , N_{Mn^-} does not increase any further but shows saturated behavior. Magnetization measurements for samples in this region revealed the formation of ferromagnetic MnAs second phase [23]. From these observations, we conclude that saturated N_{Mn^-} value in $N_{Mn} \geq 3 \times 10^{18}$ (squares with crosses in Fig. 3) is due to the precipitation of MnAs.

As to the low T_s (Ga,Mn)As samples, the relation between N_{Mn} and N_{Mn^-} can be classified into three different regions. The first region is defined by $N_{Mn} \leq 10^{18}$ cm^{-3} in which the N_{Mn^-} value is significantly lower than the N_{Mn} value. In this region, incorporated Mn acceptors are compensated by donors of some sort. One likely source is excess As incorporated during the epitaxial growth at low T_s [24]. The second region is defined by $N_{Mn} = \text{mid } 10^{18} - 10^{20}$ cm^{-3} in which N_{Mn^-} increases with N_{Mn} with the relation $N_{Mn^-} \approx N_{Mn}$. This is consistent with the presently accepted picture [5, 6] in that Mn atoms are incorporated substitutionally in the group III sub-lattice sites. As to the carrier transport, however, we infer that impurity conduction is the dominant mechanism in this region, rather than the conduction due to delocalized holes. This point will be discussed in the next section. The third region is defined by $N_{Mn} \geq 2 \times 10^{20}$ cm^{-3} in which N_{Mn^-} begins to saturate. Within the limit of this study, ferromagnetic MnAs second phase was not detected in low T_s samples even with the highest N_{Mn} of 1.5×10^{21} cm^{-3} . This fact indicates that the saturation behavior in the third region is not due to the MnAs precipitates, but is attributed to other microscopic origins, such as interstitial Mn, excess As incorporation [2, 25], and Mn-Mn dimers [26]. The first and second phenomena are believed to result in the formation of deep donors whereas

the third one might result in inert acceptor complex. Very recently, the presence of interstitial Mn has been detected by the Rutherford backscattering experiments [27].

It should be noted that the samples in the third region exhibit ferromagnetic order at low temperatures. Curie temperatures T_c of those samples ($T_c = 30-60$ K), however, do not follow the empirical formula T_c [K] = $2000 \times x (= 9 \times 10^{-20} \times N_{Mn})$ established in ref.25, but rather show a weak N_{Mn} dependence. When N_{Mn^-} is used instead of N_{Mn} , we find that experimental T_c matches with this formula. For samples with higher T_c , we notice that discrepancy between N_{Mn} and N_{Mn^-} becomes smaller. These facts indicate that the discrepancy appearing in the third region is sample dependent and can be interpreted as the quality of samples.

C. Relation between N_{Mn^-} and p

We now discuss the relationship between N_{Mn^-} and hole concentration p . Those quantities are plotted together as a function of N_{Mn} in Figs. 4(a) and (b) for high and low T_s samples, respectively. Open and closed squares respectively represent N_{Mn^-} and p for high T_s samples (Fig. 4(a)), whereas open and closed circles respectively depict N_{Mn^-} and p for low T_s samples (Fig. 4(b)). Squares with crosses and closed diamonds represent N_{Mn^-} and p for high T_s samples containing MnAs, respectively (Fig. 4(a)). The data obtained for p -GaAs:Be samples, as represented by open and closed triangles, are also plotted in Fig. 4(a) for comparison. The data obtained from Hall effect measurements for representative samples are summarized in Table 1 together with T_s , N_{Mn} , N_{Mn^-} , and T_c values. For p -GaAs:Be samples (Fig. 4(a)), it is clear that N_{Be^-} values coincide with both N_{Be} and p up to very high doping concentration, reflecting the fully ionized condition in both depletion and neutral regions because of the shallow acceptor level of Be [28]. On the other hand, for high T_s GaAs:Mn samples, p is always lower than N_{Mn^-} (Fig. 4(a)). This discrepancy can be understood in term of relatively deep acceptor level of Mn. In the depletion region where Fermi level E_F is far above E_A , Mn acceptors are fully ionized, whereas, in the neutral region where E_F is relatively closer to E_A , they are partially ionized. In fact, putting the experimental data in eq.(4a) and (4b), we obtain $E_A = 50 - 60$ meV together with $E_F = 108$ and 85 meV above the top of the valence band for samples with $N_{Mn} = 2 \times 10^{17}$ and 6×10^{17} cm^{-3} , respectively. The E_A values estimated in this fashion are consistent with earlier works in which $E_A = 60 - 80$ meV for 10^{17-18} cm^{-3} [8, 9]. This fact indicates that anomalous Hall effect is negligibly small in high T_s , Mn-doped samples. As to the p -type samples containing MnAs, the relation between N_{Mn^-} and p can also be understood in terms of Fermi distribution eq.(4a). Influence of MnAs on electronic property is not significant in these samples. Let us now turn into (Ga,Mn)As samples prepared at low T_s . In view of magneto-transport characteristics, samples are again classified into three different regions. The first region is defined by $N_{Mn} \leq 10^{18}$ cm^{-3} in which samples are highly resistive, making it difficult to extract p from Hall effect. The second region lies between N_{Mn}

TABLE I: Summary of N_{Mn} (N_{Be}), N_{Mn^-} (N_{Be^-}), resistivity ρ , hole concentration p , and mobility μ_p , together with sample ID number, substrate temperature T_s and Curie temperature T_c . It is interesting to note that actual mobility would become three to five times lower than the Hall mobility if we use N_{Mn^-} as actual p values for magnetic samples (MM142 and M66).

Sample No.	T_s (C)	N_{Mn} or N_{Be} (cm^{-3})	N_{Mn^-} or N_{Be^-} (cm^{-3})	T_c (K)	ρ ($\Omega\cdot\text{cm}$)	p (cm^{-3})	μ_p ($\text{cm}^2/\text{V}\cdot\text{s}$)
MM140 (Mn)	580	2.0×10^{17}	2.4×10^{17}	-	0.18	1.4×10^{17}	259
MM153 (Mn)	580	5.0×10^{19}	2.0×10^{18}	-	0.058	4.6×10^{17}	231
M105 (Be)	580	5.0×10^{19}	4.2×10^{19}	-	0.0017	5.0×10^{19}	70.1
MM142 (Mn)	250	1.5×10^{20}	1.4×10^{20}	30	0.019	4.4×10^{19}	7.31
M66 (Mn)	250	9.2×10^{20}	2.4×10^{20}	55	0.011	4.2×10^{19}	14.0

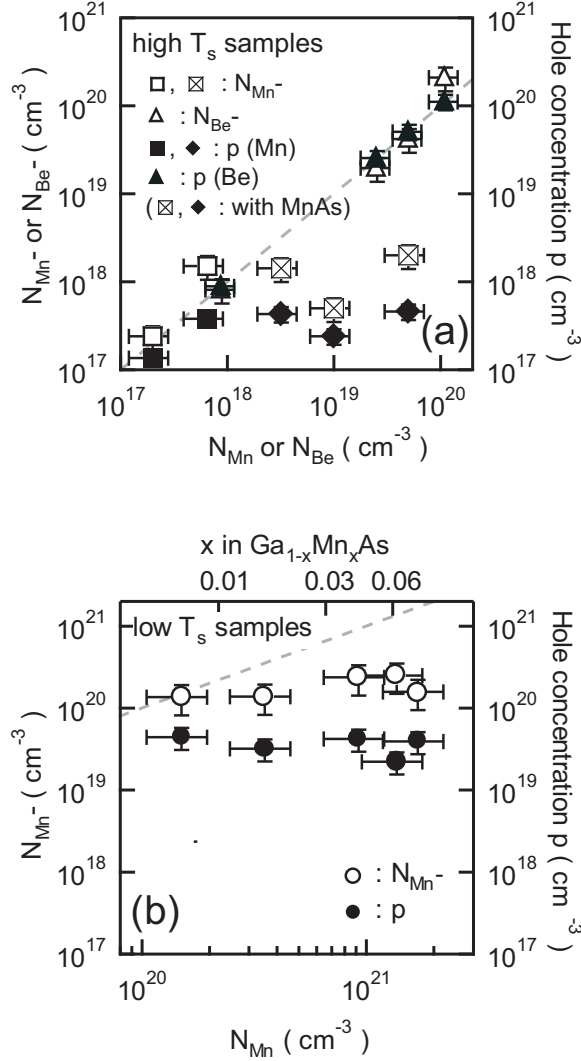


FIG. 4: N_{Mn^-} (N_{Be^-}) and p shown as a function of N_{Mn} (N_{Be}) for samples grown at (a) $T_s = 580$ C (high T_s samples) and (b) $T_s = 250$ C (low T_s samples). In Fig.4(a), \square and \triangle respectively represent N_{Mn^-} and p values for homogeneous samples, whereas \boxtimes and \boxtriangle represent N_{Mn^-} and p for samples containing MnAs, respectively. In Fig.4(b), \circ and \bullet respectively depict N_{Mn^-} and p for magnetic (Ga,Mn)As samples. The data obtained for p -GaAs:Be samples, as represented by ϕ and ϵ , are also plotted for comparison.

= mid 10^{18} and 10^{20} cm^{-3} in which samples are conductive but show virtually zero Hall resistance at room temperature (RT) as well as at 77 K. In conventional high T_s GaAs:Mn samples with $N_{Mn} \approx 10^{19}$ cm^{-3} , similar behavior has been observed at low temperatures (< 75 K), and has been discussed in terms of impurity conduction [9]. Knowing that, for high T_s samples, MnAs precipitation occurs at around 3×10^{18} cm^{-3} beyond which N_{Mn^-} saturates (Fig. 3), the effective N_{Mn} that causes the impurity conduction is inferred to be slightly above 3×10^{18} cm^{-3} . It is also inferred that, if effective N_{Mn^-} is increased, the conductivity due to impurity conduction increases so that the temperature that causes a cross-over from impurity conduction to delocalized-band conduction shifts toward high temperatures. We believe that this is what has been observed for low T_s samples with $N_{Mn} = \text{mid } 10^{18} - 10^{20}$ cm^{-3} . Consequently, the second region can be treated as an extended region beyond $N_{Mn} = \text{mid } 10^{18}$ cm^{-3} of high T_s samples with $N_{Mn} = N_{Mn^-} = p$. For low T_s samples, impurity conduction dominates even at RT, reflecting the very high N_{Mn} values.

The third region is defined by $N_{Mn} \geq 2 \times 10^{20}$ cm^{-3} in which samples are sufficiently conductive and exhibit finite, positive Hall resistance. Results are shown in Fig. 4(b) and Table I. As discussed in the previous paragraph, impurity band is formed $N_{Mn} \sim \text{mid } 10^{18}$ cm^{-3} or higher. When N_{Mn} is increased further, the overlap of wavefunction becomes more and more significant, causing an increase in impurity band width. At some point, the impurity band overlaps with top of the valence band, resulting in charge transfer between the two bands. Under this situation, carrier transport occurs through the delocalized valence band mixed with the impurity band and thus revival of the Hall effect. Based on our experimental results, the overlap between the two bands seems to occur at around $N_{Mn} \sim 2 \times 10^{20}$ cm^{-3} . Within the limit of this scenario, it is reasonable to assume that the number of carriers p is equal to N_{Mn^-} , being similar to the second region. However, experimentally, we notice that p obtained from Hall effect is lower than N_{Mn^-} in the third region ($N_{Mn} > N_{Mn^-} > p$). Finally, we come to the point that the anomalous Hall effect is likely to give rise to the discrepancy between p and N_{Mn^-} in this region.

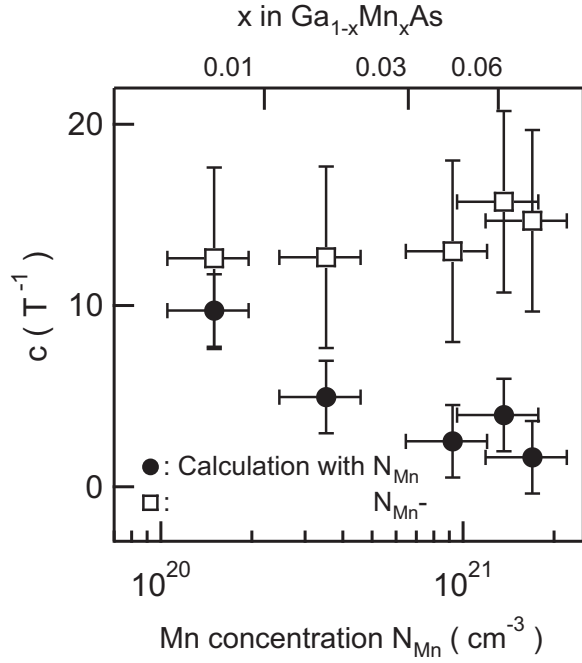


FIG. 5: A plot of asymmetric scattering constant c vs. incorporated Mn concentration N_{Mn} .

D. Asymmetric scattering constant c

To pursue further, we have calculated the asymmetric scattering constant c by using eqs.(2), (3a) and (3b). This is the estimation of c at room temperature for the first time. The experimental value obtained from the Hall effect measurements was substituted directly for R_H in the left hand side of eq.(2). The first term in the right hand side of eq.(2) was estimated from eq.(3a) by substituting experimental N_{Mn^-} value obtained from $C - V$ measurements for p . The anomalous Hall term can then be obtained, and it is substituted for the left hand side of the eq.(3b). In eq.(3b), perpendicular magnetization M at room temperature is estimated from the calculated magnetic susceptibility c based on the Curie-Weiss law $\chi = C/(T - \theta_p)$ with $C = N_{Mn}g^2\mu_B^2\{S(S + 1)\}/3k$. Here, paramagnetic Curie temperature θ_p is assumed to be equal to the Curie temperature, whereas spin number S and g factor are $S = 5/2$ and $g = 2$, respectively. $n = 1$ in eq.(3b) because skew scattering is believed to be dominant in (Ga,Mn)As [3]. It is very important to notice that the constant c extracted in this fashion from eq.(3b) can be influenced significantly by the definition of Mn atoms that is responsible for c at RT. There are two possibilities to estimate c ; either using the total concentration N_{Mn} or using the concentration of ionized Mn acceptors N_{Mn^-} . The c values calculated for both cases are shown in Fig. 5, from which we notice an interesting difference between the two cases. When N_{Mn} is used, we obtain c values that range between 1 and 10 and are nearly inversely

proportional to N_{Mn} . In contrast, in case of N_{Mn^-} , we find a fixed value of $c = 13 \pm 5$ independent of the N_{Mn^-} . Since the range of Mn concentration is low enough to neglect the scattering processes of higher orders, we believe that c should in principle be independent of N_{Mn^-} (and N_{Mn} as well). Consequently, the results based on N_{Mn^-} seem to grab the essential physics in magnetic (Ga,Mn)As. Previously, the asymmetric scattering constant was estimated to be $c = 2$ for $\text{Ga}_{1-x}\text{Mn}_x\text{As}$ with $x = 0.035$ by comparing magnetization and Hall resistance data in ferromagnetic phase [3]. In ferromagnetic p -(In,Mn)As, the c value has been estimated to be $c = 6$ for $x = 0.013$ [29]. That the c value extracted in this work is larger than the values extracted in previous works may come from the use of the N_{Mn^-} instead of N_{Mn} . This point should be examined in the future work by carefully evaluating magnetization data and transport data for wide range of temperature.

IV. CONCLUSIONS

Determination of N_{Mn} , N_{Mn^-} , and p has been carried out for Mn-doped GaAs epitaxial layers with wide range of Mn concentrations ($10^{17} - 10^{21} \text{ cm}^{-3}$). Key experiment in this study was electrochemical $C - V$ method by which N_{Mn^-} has been extracted successfully. Carefully comparing N_{Mn^-} with N_{Mn} and p , several important conclusions have been deduced. For high T_s samples, Mn starts to precipitate in the form of MnAs when N_{Mn} becomes higher than about $3 \times 10^{18} \text{ cm}^{-3}$. Except this point, electronic behavior of the high T_s epilayers is not affected by the MnAs inclusions, and is essentially the same as those studied in 70's. For low T_s samples, electronic behaviors can be classified into three different regions. The first region is highly resistive, strongly compensated region in $N_{Mn} \leq 10^{18} \text{ cm}^{-3}$. The second region is impurity conduction region in $N_{Mn} = \text{mid } 10^{18} - 10^{20} \text{ cm}^{-3}$ with $N_{Mn} \approx N_{Mn^-}$, which can be regarded as the extended region of high T_s epilayers of N_{Mn} beyond mid 10^{18} cm^{-3} . The third region, defined by $N_{Mn} \geq 2 \times 10^{20} \text{ cm}^{-3}$, is the region having characteristics similar to the electrical conduction due to delocalized holes. In this region, magnetism and carrier transport are strongly correlated to each other, causing ferromagnetism and anomalous Hall effect. Quantitative assessment of anomalous Hall effect at room temperature has been carried out, from which asymmetric scattering constant c is determined to be $c = 13 \pm 5$ at room temperature.

Acknowledgments

We gratefully acknowledge S. Kikuchi for technical assistance. This work is supported in part by Scientific Research in Priority Areas "Semiconductor Nanospintronics" of The Ministry of Education, Culture, Sports, Science and Technology, Japan.

-
- [1] H. Munekata, H. Ohno, S. von Molnar, A. Segmuller, L. L. Chang and L. Esaki, Phys. Rev. Lett. **63**, 1849 (1989).
- [2] H. Munekata, H. Ohno, R. R. Ruf, R. J. Gambino and L. L. Chang, J. Cryst. Growth **111**, 1011 (1991).
- [3] H. Ohno, A. Shen, F. Matsukura, A. Oiwa, A. Endo, S. Katsumoto and Y. Iye, Appl. Phys. Lett. **69**, 363 (1996).
- [4] T. Hayashi, M. Tanaka, T. Nishinaga, H. Shimada, H. Tsuchiya and Y. Ohtsuka, J. Cryst. Growth **175/176**, 1063 (1997).
- [5] see for e.g., H. Ohno, J. Magn. Magn. Mater. **200**, 110 (1999).
- [6] Y. L. Soo, S. W. Huang, Z. H. Ming, Y. H. Kao, H. Munekata and L. L. Chang, Phys. Rev. B **53**, 4905 (1996).; R. Shioda, K. Ando, T. Hayashi and M. Tanaka, Phys. Rev. B **58**, 1100 (1998).
- [7] M. Ilegems, R. Dingle, and L.W. Rupp Jr., J. Appl. Phys. **46**, 3059 (1975).
- [8] J. S. Blakemore, Winfield J. Brown Jr., Merrill L. Stass, and Dustin A. Woodbury J. Appl. Phys. **44**, 3352 (1973).
- [9] Dustin A. Woodbury, J. S. Blakemore, Phys. Rev. B **8**, 3803 (1973).
- [10] A. Oiwa, S. Katsumoto, A. Endo, M. Hirasawa, Y. Iye, H. Ohno, F. Matsukura, A. Shen and Y. Sugawara, Solid State Commun. **103**, 209 (1997).
- [11] T. Dietl, H. Ohno and F. Matsukura, Phys. Rev. B **63**, 195205 (2001).
- [12] K. M. Yu, W. Walukiewicz, T. Wojtowicz, W. L. Lim, X. Liu, Y. Sasaki, M. Dobrowolska, and J. K. Furdyna, Appl. Phys. Lett. **81**, 844 (2002).
- [13] X.Liu, A. Prasad, J. Nishio, E. R. Weber, Z. Liliental-Weber and W. Walukiewicz, Appl. Phys. Lett. **67**, 279 (1995).
- [14] R. E. Honig and D. A. Kramer, RCA Review **30**, 285 (1969).
- [15] P. Blood, Semicond. Sci. Technol. **1**, 7 (1986).
- [16] S. M. Sze, Physics of Semiconductor Devices, 2nd ed. (Wiley, New York, 1981), p. 245.
- [17] L. J. van der Pauw, Philips Reserch Reports **13**, 1 (1958).
- [18] T. R. McGuire, R. J. Gambino and R. C. O'Handley, in The Hall effect and Its Applications, edited by C. L. Chien and C. R. Westgate (Plenum Press, New York, 1980), p. 149.
- [19] T. Omiya, F. Matsukura, T. Dietl, Y. Ohno, T. Sakon, M. Motokawa, and H. Ohno, Physica E **7**, 976 (2000).
- [20] R. A. Smith, Semiconductors, 2nd ed. (Cambridge University Press, Cambridge, 1978), p. 86.
- [21] C. Yamanouchi, K. Mizuguchi and W. Sasaki, J. Phys. Soc. Japan **22**, 859 (1967).
- [22] V. W. L. Chin, M. A. Green, J. W. V. Storey, J. Appl. Phys. **68**, 3470 (1990).; J. R. Waldrop, J. Vac. Sci. Technol. B **2**, 445 (1984).
- [23] a hysereitic $M - H$ curve with saturation magnetization of 3×10^{-7} emu was detected in a high T_s GaAs:Mn sample with $N_{Mn} = 3 \times 10^{18}$ cm⁻³. About 40 % of Mn is incorporated in the form of MnAs second phase.
- [24] D. C. Look, J. Appl. Phys. **70**, 3148 (1991).
- [25] F. Matsukura, H. Ohno, A. Shen and Y. Sugawara, Phys. Rev. B **57**, R2037 (1998).
- [26] T. Slupinski, A. Oiwa, S. Yanagi, H. Munekata, J. Cryst. Growth **237/239**, 1326 (2002).
- [27] K. M. Yu, W. Walukiewicz, T. Wojtowicz, I. Kuryliszyn, X. Liu, Y. Sasaki and J. K. Furdyna, Phys. Rev. B **65**, 201303 (2002).
- [28] Pallab K. Chatterjee, K. V. Vaidyanathan, W. V. McLevige and B. G. Streetman, Appl. Phys. Lett. **27**, 567 (1975).
- [29] H. Ohno, H. Munekata, T. Penney, S. von Molnar, and L.L. Chang, Phys. Rev. Lett. **68**, 2664 (1992).